Werk

Jahr: 1975
Kollektion: fid.geo
Signatur: 8 Z NAT 2148:41
Digitalisiert: Niedersächsische Staats- und Universitätsbibliothek Göttingen
Werk Id: PPN1015067948_0041
PURL: http://resolver.sub.uni-goettingen.de/purl?PPN1015067948_0041

LOG Id: LOG_0069
LOG Titel: Synthetic seismograms of PS-reflections from transition zones computed with the reflectivity method
LOG Typ: article

Übergeordnetes Werk

Werk Id: PPN1015067948
PURL: http://resolver.sub.uni-goettingen.de/purl?PPN1015067948
OPAC: http://opac.sub.uni-goettingen.de/DB=1/PPN?PPN=1015067948

Contact

Niedersächsische Staats- und Universitätsbibliothek Göttingen
Georg-August-Universität Göttingen
Platz der Göttinger Sieben 1
37073 Göttingen
Germany
Email: gdz@sub.uni-goettingen.de

J. Geophys. 41, 445–462, 1975

Original Investigations

Synthetic Seismograms of PS-Reflections from Transition Zones Computed with the Reflectivity Method*

K. Fuchs

Geophysikalisches Institut, Universität Karlsruhe

Abstract. Expressions for the computation of synthetic seismograms of *PS*-reflections from transition zones with an arbitrary depth-dependent distribution of the elastic moduli and density are derived by the reflectivity method. Synthetic seismograms of *PS*-reflections are presented for first-order discontinuities with variable Poisson's ratio, for linear transition zones with variable thickness, and for laminas of variable thickness. The computed theoretical amplitudes show that from a crust-mantle boundary with a first-order discontinuity *PS*-reflections should be observable. However, in most crustal explosion studies *PS*-reflections are not observed, as demonstrated in a number of record sections. Both, transition zones and a reduction of *S*-wave velocity in the lower halfspace diminish the amplitudes of supercritically reflected *PS*-waves without affecting the amplitudes of the supercritical *PP*-reflection. On supercritical reflection from thin laminas both *PP* and *PS* amplitudes decrease. A transition zone is the most likely explanation of the observed absence of reflected *PS*-waves from the crust-mantle boundary. Its thickness should be at least 1 km.

Key words: *PS*-reflections – Synthetic seismograms – Reflectivity method – Crust-mantle boundary – Variable poisson's ratio – Linear transition zone – Lamina.

1. Introduction

Explosion seismology has concentrated almost exclusively on the interpretation of *P*-waves for two reasons. Firstly explosions are radiating dominantly compressional waves; and, secondly, the *P*-waves form the first arriving group, where in general arrival times can be picked much more reliably than in the case of the later arriving *S*-waves. However, there are quite a number of record sections

* Contribution No. 181 within a joint research program of the Geophysical Institutes in Germany sponsored by the Deutsche Forschungsgemeinschaft (German Research Association). Contribution No. 104, Geophysikalisches Institut Universität Karlsruhe.

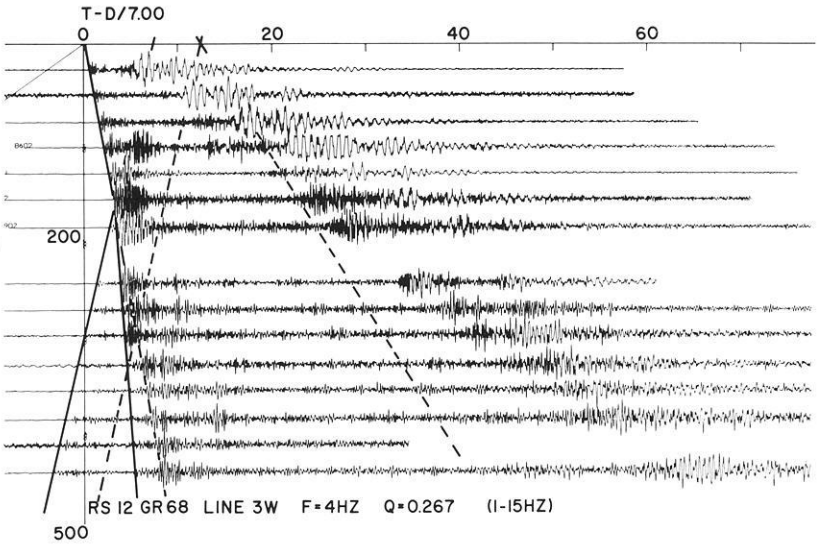

Fig. 1. Record section from profile Greenville 3 *W* in Canada. Reduction velocity 7.0 km/s. The dashed lines indicate the theoretical positions of the S_n and PPS-headwaves corresponding to the P_n-branch (adapted from Berry and Fuchs, 1973). Note the presence of the $S_M S$ phase and the absence of observable PPS- and PS-phases

available from explosion seismic experiments in various parts of the globe where *S*-phases show amplitudes comparable with the corresponding *P*-phases (Figs. 1–2). These *S*-phases must have been radiated directly from the source or converted immediately from *P*-waves in the neighbourhood of the source. These examples prove that *S*-waves are propagated with sufficient energy through the crust in the frequency range of explosion seismic experiments. Therefore, the question arises whether *PS*-reflections converted at transition zones in the crust and upper mantle can also be observed.

The reduced traveltime diagram for *PP*- and *PS*-reflections from the crust-mantle boundary of a one-layer crust is given in Fig. 4. At this first-order discontinuity the *P*-wave in the upper mantle is guiding a *P*-headwave (*PPP*) and a *S*-headwave (*PPS*). The critical distance (49.6 km) of the *PPS*-phase is nearly 20 km smaller than that for the *PPP*-phase (69.3 km). The time lag between *PPS* and *PPP* is 4.4 sec. The *PPS*-headwave is tangent to the converted $P_M S$-reflection. The asymptotic velocity of the $P_M S$-reflection at large distances becomes α_1 which is identical with the *P*-velocity of the crust, this is the same asymptotic velocity as that of the $P_M P$ reflection.

The approximate position of the *PPS*-traveltime branch is reproduced in the record sections of Figs. 1–3. It is quite evident that no energy comparable to the critical $P_M P$- or $S_M S$-reflection is present in these sections. The absence of $P_M S$-reflections appears to be a general feature of crustal record sections.

It is the purpose of this paper to investigate possible reasons for the observed absence of *PS*-reflections from the crust-mantle boundary. In the first part the reflectivity method (Fuchs, 1968b; Fuchs and Müller, 1971) is extended to include

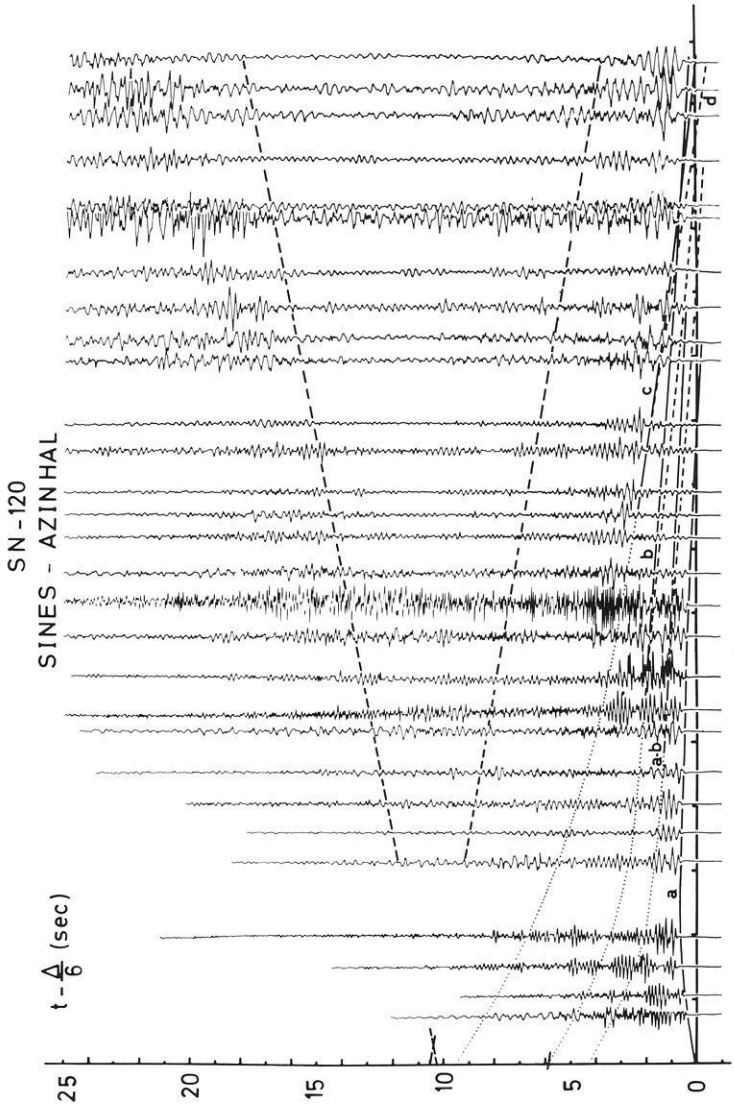

Fig. 2. Record section from profile Sines-Azinhal in Portugal. Reduction velocity 6.0 km/s. Dashed line indicates the theoretical position of the S_n and PPS headwaves corresponding to the P_n-branch (adapted from Müller *et al.*, 1973). Note the presence of the S_MS-phase and the absence of observable PPS- and PS-phases

the computation of synthetic PS-seismograms. In the second part PS-reflections from various kinds of transition zones will be presented which are likely candidates for the suppression of PS-reflections.

2. The Computation of Synthetic *PS*-Seismograms with the Reflectivity Method

The method for the computation of synthetic PP-seismograms with the reflectivity method (Fuchs, 1968 b) had been extended by Fuchs and Müller (1971) to cover the case of an arbitrary stack of horizontal layers on top of the reflecting zone. Here we will use the same notation as in this paper. The model of the layered medium is given in Fig. 5. It consists of $n-1$ plane, horizontal, homogeneous,

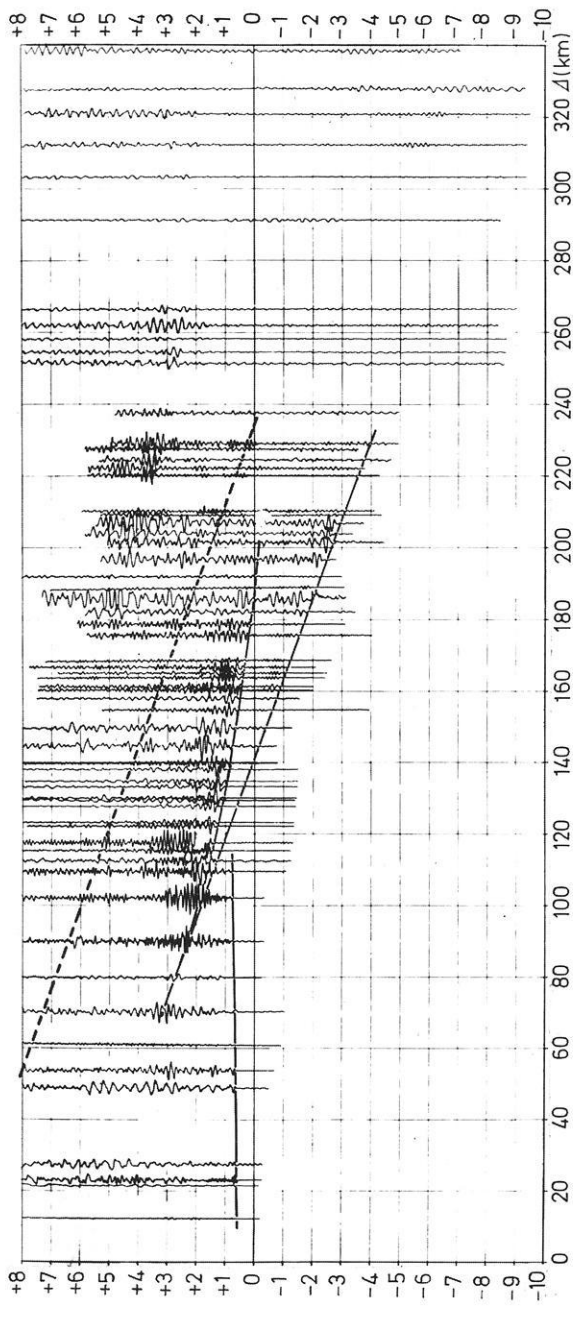

Fig. 3. Record section from profile Hilders-south in F. R. Germany. Reduction velocity 6.0 km/s. Dashed line indicates theoretical position of *PPS* headwave corresponding to the P_n-branch (adapted from Kaminski *et al.*, 1967). Note the absence of observable *PPS*- and *PS*-phases

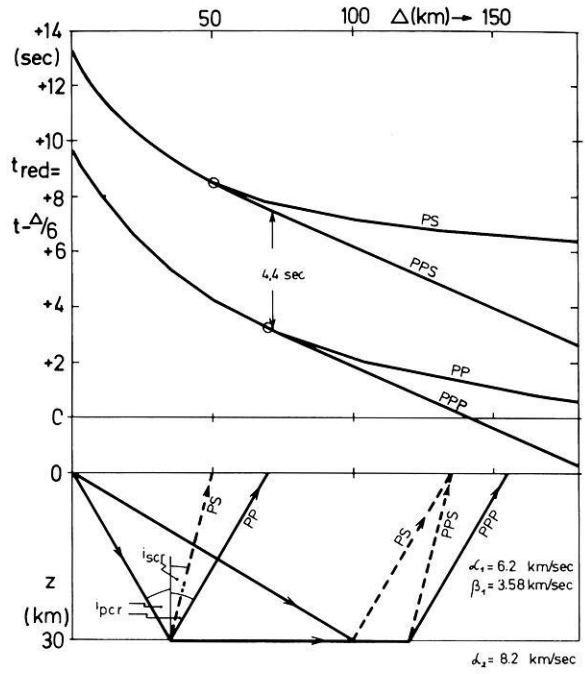

Fig. 4. Reduced traveltime diagram for *PP*- and *PS*-reflections from the base of a one-layer crust with schematic ray-paths

and isotropic layers on top of the half-space (layer n). The i-th layer is characterized by the P-velocity α_i, S-velocity β_i, density ρ_i; and thickness h_i. The explosive point source is placed in the free surface at $z=0$ without taking into account an interaction, *i.e.*, the P-waves in layer 1 are spherically symmetric and no S-waves are excited. In the layers 1 through m only transmission losses and traveltime delays of P- and S-waves are considered, multiple reflections within these m layers are neglected. The reflecting zone is formed by the layers $m+1$ through n. From the source to the top of the reflecting zone and back to the surface the exact or generalized ray theory (Müller, 1968a, b; 1970) will be followed while the reflection from the transition zone is described by the reflectivity method.

The compressional potential of the wave radiated from the explosive point source into layer 1 is:

$$\varphi_0(r, z, t)=\frac{1}{R}\cdot F\left(t-\frac{R}{\alpha_1}\right). \tag{1}$$

Where $R^2=r^2+z^2$. Its Fourier transform is in integral form:

$$\bar{\varphi}_0(r, z, \omega)=\bar{F}(\omega)\int_0^{\infty}\frac{k}{j\nu_1}\cdot J_0(kr)\exp(-j\nu_1 z)\,dk. \tag{2}$$

Here $\bar{F}(\omega)$ is the Fourier transformed source function $F(t)$, $J_0(kr)$ the Bessel function of the first kind and order zero, j the imaginary unit, k the horizontal

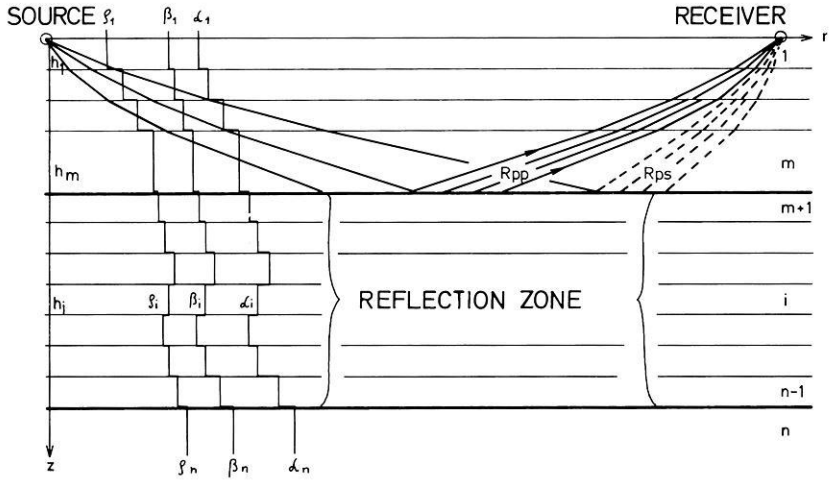

Fig. 5. Model of the layered medium with the position of the source and the receiver at the surface. The reflected *P*- and *S*-waves suffer elastic transmission losses and time delays in the layers 1 to *m*

wave number. The vertical wave numbers for *P* and *S* waves in the *i*-th layer are:

$$\nu_i=(k_{\alpha_i}^2-k^2)^{1/2}; \qquad \nu_i'=(k_{\beta_i}^2-k^2)^{1/2} \tag{3}$$

with:

$$k_{\alpha_i}=\omega/\alpha_i; \qquad k_{\beta_i}=\omega/\beta_i.$$

Transmitting this potential through the refracting layers of the overburden, the compressional potential of the *P*-wave in layer *m*, incident upon the reflecting zone, is:

$$\bar{\varphi}_1(r,z,\omega)=\bar{F}(\omega)\int_0^{\infty}\frac{k}{j\nu_1}J_0(kr)\cdot P_d(\omega,k)$$
$$\cdot\exp\left[-j\left(\sum_{i=1}^{m-1}h_i\nu_i+\left(z-\sum_{i=1}^{m-1}h_i\right)\nu_m\right)\right]dk \tag{4}$$

where $P_d(\omega,k)$ is the product of the transmission coefficients at the interfaces 2 through *m* for downward propagation of a *P*-wave.

So far we have followed the formulation of Fuchs and Müller (1971) who computed the *PP*-reflection from the transition zone. In addition to the *PP*-phase, in general, the transition zone reflects also *S*-waves whose potential in the *m*-th layer is:

$$\bar{\psi}_2(r,z,\omega)=\bar{F}(\omega)\int_0^{\infty}\frac{k}{\nu_1}J_1(kr)\cdot P_d(\omega,k)\cdot\tilde{R}_{PS}(\omega,k)$$
$$\cdot\exp\left[-j\left(\sum_{j=1}^{m}h_i\nu_i+\left(\sum_{i=1}^{m}h_i-z\right)\nu_m'\right)\right]dk. \tag{5}$$

The complex reflectivity $\tilde{R}_{PS}(\omega,k)$ of the reflecting zone is the same as defined by Fuchs (1968a), $J_1(kr)$ is the Bessel function of the first kind and first order.

The reflected wave is now propagated upwards through the interfaces m, $m-1, \ldots, 2$. Its potential in layer 1 is:

$$\bar{\psi}_3(r,z,\omega)=\bar{F}(\omega)\int_0^\infty \frac{k}{v_1} J_1(kr)\cdot P_d(\omega,k)\cdot S_u(\omega,k)\cdot \tilde{R}_{PS}(\omega,k)$$
$$\cdot\exp\left[-j\left(\sum_{i=1}^{m} h_i(v_i+v_i')-z\cdot v_i'\right)\right]dk \tag{6}$$

S_u is the product of transmission coefficients of the upward travelling S-wave at the interfaces $m, m-1, \ldots, 2$.

While the effect of the free surface has been neglected at the source it will be taken into account at the receiver. At the incidence of the S-wave upon the free surface a S- and a P-wave is reflected with potentials:

$$\bar{\psi}_4(r,z,\omega)=\bar{F}(\omega)\int_0^\infty \frac{k}{v_1} J_1(kr)\, P_d(\omega,k)\cdot S_u(\omega,k)\cdot \tilde{R}_{PS}(\omega,k)\cdot r_{ss}(\omega,k)$$
$$\cdot\exp\left[-j\left(\sum_{i=1}^{m} h_i(v_i+v_i')+z\cdot v_1'\right)\right]dk, \tag{7}$$

$$\bar{\varphi}(r,z,\omega)=\bar{F}(\omega)\int_0^\infty \frac{k}{jv_1} J_0(kr)\, P_d(\omega,k)\cdot S_u(\omega,k)\,\tilde{R}_{PS}(\omega,k)\cdot r_{sp}(\omega,k)$$
$$\cdot\exp\left[-j\left(\sum_{i=1}^{m} h_i(v_i+v_i')+z\cdot v_1'\right)\right]dk \tag{8}$$

$r_{ss}(\omega,k)$ and $r_{sp}(\omega,k)$ are the $S-S$ and $S-P$ reflection coefficients at the free surface.

The horizontal and vertical displacement in the first layer are:

$$\bar{u}=\frac{\partial\bar{\varphi}}{\partial r}-\frac{\partial\bar{\psi}_3}{\partial z}-\frac{\partial\bar{\psi}_4}{\partial z},$$

$$\bar{w}=\frac{\partial\bar{\varphi}}{\partial z}+\frac{\partial\bar{\psi}_3}{\partial r}+\frac{\partial\bar{\psi}_4}{\partial r}+\frac{\bar{\psi}_3}{r}+\frac{\bar{\psi}_4}{r}.$$

For $z=0$ we derive with Eqs. (6), (7) and (8):

$$\bar{u}(r,0,\omega)=\bar{F}(\omega)\int_0^\infty \frac{jk^2}{v_1} J_1(kr)\, P_d(\omega,k)\cdot S_u(\omega,k)\cdot \tilde{R}_{PS}(\omega,k)$$
$$\cdot\left[r_{sp}-\frac{v_1'}{k}(1-r_{ss})\right]\cdot\exp\left[-j\sum_{i=1}^{m} h_i(v_i+v_i')\right]dk, \tag{9}$$

$$\bar{w}(r,0,\omega)=\bar{F}(\omega)\int_0^\infty \frac{k^2}{v_1} J_0(kr)\cdot P_d(\omega,k)\cdot S_u(\omega,k)\cdot \tilde{R}_{PS}(\omega,k)$$
$$\cdot\left[1+r_{ss}-\frac{v_1}{k}r_{sp}\right]\cdot\exp\left[-j\sum_{i=1}^{m} h_i(v_i+v_i')\right]dk. \tag{10}$$

For numerical integration it has been found more convenient to use the angle γ as new variable, related to k by:

$$k=\frac{\omega}{\alpha_m}\sin\gamma=k_{\alpha_m}\sin\gamma. \tag{11}$$

For $k\leqq k_{\alpha_m}$ γ is the real angle of incidence in the m-th layer at the top of the reflecting zone. With the new variable γ the coefficients P_d, S_u, r_{ss} and r_{sp} depend only on γ. The integrals (9) and (10) become:

$$\bar{u}(r,0,\omega)=\bar{F}(\omega)\cdot k_{\alpha_m}^2\int_{\gamma_1}^{\gamma_2}\sin\gamma\cos\gamma j\cdot J_1(k_{\alpha_m}r\sin\gamma)\,\tilde{R}_{PS}(\omega,\gamma)\cdot A(\gamma)$$
$$\cdot\exp\left[-jk_{\alpha_m}\sum_{i=1}^{m}h_i(\eta_i+\eta_i')\right]d\gamma, \tag{12}$$

$$\bar{w}(r,0,\omega)=\bar{F}(\omega)\cdot k_{\alpha_m}^2\int_{\gamma_1}^{\gamma_2}\sin\gamma\cos\gamma\cdot J_0(k_{\alpha_m}r\sin\gamma)\,\tilde{R}_{PS}(\omega,\gamma)\cdot B(\gamma)$$
$$\cdot\exp\left[-jk_{\alpha_m}\sum_{i=1}^{m}h_i(\eta_i+\eta_i')\right]d\gamma \tag{13}$$

where

$$A(\gamma)=a(\gamma)\cdot P_d(\gamma)\cdot S_u(\gamma)\quad\text{and}\quad B(\gamma)=b(\gamma)\cdot P_d(\gamma)\cdot S_u(\gamma) \tag{14}$$

and

$$a(\gamma)=\frac{\nu_1'}{\nu_1}\left[1-r_{ss}-\frac{k}{\nu_1'}r_{sp}\right], \tag{15}$$

$$b(\gamma)=\frac{k}{\nu_1}\left[1+r_{ss}-\frac{\nu_1}{k}r_{sp}\right]. \tag{16}$$

The products of the transmission coefficients P_d and S_u are:

$$P_d=\prod_{i=2}^{m}T_{ppi}(\gamma)\quad\text{and}\quad S_u=\prod_{i=2}^{m}T_{ssi}(\gamma) \tag{17}$$

where:

$$T_{ppi}(\gamma)=-2\rho_{i-1}\cdot\eta_{i-1}\frac{C}{D},$$

$$T_{ssi}(\gamma)=-2\rho_i\eta_i'\frac{\bar{C}}{D}$$

with:

$$C=\eta_i'(d_i\sin^2\gamma-\rho_{i-1})-\eta_{i-1}'(d_i\sin^2\gamma+\rho_i),$$
$$\bar{C}=\eta_i(d_i\sin^2\gamma-\rho_{i-1})-\eta_{i-1}(d_i\sin^2\gamma+\rho_i),$$

$$D=\sin^2\gamma(d_i\sin^2\gamma+\rho_i-\rho_{i-1})^2+\eta_i\eta_i'(d_i\sin^2\gamma-\rho_{i-1})^2$$
$$+\rho_{i-1}\rho_i\eta_i\eta_{i-1}'+\eta_{i-1}[d_i^2\eta_i\eta_{i-1}'\eta_i'\sin^2\gamma$$
$$+\eta_{i-1}'(d_i\sin^2\gamma+\rho_i)^2+\rho_{i-1}\rho_i\eta_i'], \tag{18}$$
$$\eta_i=\left[\left(\frac{\alpha_m}{\alpha_i}\right)^2-\sin^2\gamma\right]^{1/2},\quad \eta_i'=\left[\left(\frac{\alpha_m}{\beta_i}\right)^2-\sin^2\gamma\right]^{1/2}.$$

The coefficients $a(\gamma)$ and $b(\gamma)$ are:

$$a(\gamma)=-\frac{1}{N}\frac{\eta_1'}{\eta_1}\cdot\frac{\alpha_m^2}{\beta_1^2}\cdot 2\left(2\sin^2\gamma-\frac{\alpha_m^2}{\beta_1^2}\right),$$
$$b(\gamma)=\frac{1}{N}\cdot 4\frac{\alpha_m^2}{\beta_1^2}\eta_1'\sin\gamma, \tag{19}$$
$$N=4\sin^2\gamma\,\eta_1\eta_1'+\left(2\sin^2\gamma-\frac{\alpha_m^2}{\beta_1^2}\right)^2.$$

Without the influence of the free surface at $z=0$ the coefficients $a(\gamma)$ and $b(\gamma)$ become:

$$a(\gamma)=\frac{\nu_1'}{\nu_1}\quad\text{and}\quad b(\gamma)=\frac{k}{\nu_1}.$$

Since we are only interested in the reflection of body waves the integration in Eqs. (12) and (13) will be restricted to real angles γ, *i.e.* $0\leqq\gamma\leqq\pi/2$ as was discussed by Fuchs and Müller (1971).

For crustal explosion studies it is convenient to replace the Bessel functions by their large distance approximations:

$$J_0(x)=\sqrt{\frac{2}{\pi x}}\cos\left(x-\frac{\pi}{4}\right)$$
$$=\frac{1}{\sqrt{2\pi x}}\left\{\exp\left[j\left(x-\frac{\pi}{4}\right)\right]+\exp\left[-j\left(x-\frac{\pi}{4}\right)\right]\right\}, \tag{20}$$
$$J_1(x)=\sqrt{\frac{2}{\pi x}}\sin\left(x-\frac{\pi}{4}\right)$$
$$=\frac{-j}{\sqrt{2\pi x}}\left\{\exp\left[j\left(x-\frac{\pi}{4}\right)\right]-\exp\left[-j\left(x-\frac{\pi}{4}\right)\right]\right\}. \tag{21}$$

The first exponential term in Eqs. (20) and (21) corresponds to waves travelling towards the source. It can be shown by numerical evaluation that the contribution of these terms to the integrals in Eqs. (12) and (13) are negligible. Neglecting these terms the two integrals become:

$$\bar{u}(r,0,\omega)=-\bar{F}(\omega)\,e^{j\pi/4}\sqrt{\frac{k_{\alpha_m}^3}{2\pi r}}\int_{\gamma_1}^{\gamma_2}\sqrt{\sin\gamma}\cos\gamma\,\tilde{R}_{PS}(\omega,\gamma)\cdot E(\gamma)$$
$$\cdot\exp\left\{-jk_{\alpha_m}\left[r\sin\gamma+\sum_{i=1}^{m}h_i(\eta_i+\eta_i')\right]\right\}d\gamma, \tag{22}$$

$$\bar{w}(r,0,\omega)=\bar{F}(\omega)\,e^{j\pi/4}\sqrt{\frac{k_{\alpha_m}^3}{2\pi r}}\int_{\gamma_1}^{\gamma_2}\sqrt{\sin\gamma}\cdot\cos\gamma\,\tilde{R}_{PS}(\omega,\gamma)\cdot B(\gamma)$$
$$\cdot\exp\left\{-jk_{\alpha_m}\left[r\sin\gamma+\sum_{i=1}^{m}h_i(\eta_i+\eta_i')\right]\right\}d\gamma. \tag{23}$$

The Fortran-program "Reflexion" has been extended to include synthetic seismograms of *PS*-reflections according to Eqs. (22) and (23).

3. *PS*-Reflections from Various Kinds of Transition Zones

In this section the extended computer-program will be applied to investigate the absence of *PS*-reflections from the crust-mantle boundary on observed record sections from crustal explosion-seismic experiments. The far-field displacement of the compressional wave from the explosive source is proportional to the derivative $F'(t)$ of the source function $F(t)$. In the following examples $F'(t)$ is:

$$F'(t)=\begin{cases}\sin 10\pi t-0.5\sin 20\pi t & \text{for } 0\leqq t\leqq 0.2\text{ sec}\\ 0 & \text{for } t<0 \quad\text{and}\quad t>0.2\text{ sec}.\end{cases}$$

This signal with a duration of 0.2 sec has a dominant frequency of about 5 Hz.

3.1. PS-Reflections from a First-Order Discontinuity

A one-layer crustal model with a first-order discontinuity as crust-mantle boundary serves as a first model (Model 1 in Table 1) for which synthetic seismograms of *PS*-reflections are computed. The traveltimes for this model had been given already in Fig. 4. The *PP*- and *PS*-section of the vertical component are given separately, both on the same amplitude scale, in Fig. 6.

The phases of the reflections $P_M P$ and $P_M S$ as well as the headwaves *PPP* and *PPS* are clearly recognized. While the $P_M P$ reflection suffers a phase change of 180° at grazing incidence, that $P_M S$ reflection shows the same phase as the subcritical $P_M S$ reflection. The most important observation is that the maximum *PS*-amplitude reaches about 0.6 of the maximum *PP*-amplitude in case of a purely compressional source. Should the source radiate *S*-waves as well, the *SP* phase would constructively interfere, with the *PS* phase, and the combined *PS* and *SP* phase could attain amplitudes larger or equal to the *PP* phase. – The maximum of the *PS*-reflection does not occur at the critical distance of 49.6 km but is displaced to larger distances (63.5 km) by the interference of the *PS*-reflection and the *PPS*-headwave. This is the same effect as discussed for supercritically reflected *P*-waves by Červený (1961).

Comparing these synthetic seismograms for *PS*-reflections from a first-order discontinuity with the observed record sections of Figs. 1–3 one clearly recognizes that the observations do not show appreciable energy of arrivals at the places where the *PS*-reflection is expected. Therefore, the question arises which models of the crust-mantle boundary may cause a suppression of the *PS*-reflections. In

Table 1. Models of Transition Zones

Model	No.	Poisson's ratio	Thickness of first layer	α_1 (km/s)	β_1 (km/s)	ρ_1 (g/cm^3)	α_2 (km/s)	β_2 (km/s)	ρ_2 (g/cm^3)
First-Order Discontinuity	1	0.25	30	6.2	3.575	2.6	8.2	4.73	3.36
	2	0.30	30	6.2	3.575	2.6	8.2	4.38	3.36
	3	0.378	30	6.2	3.575	2.6	8.2	3.575	2.6
	4	0.4	30	6.2	3.575	2.6	8.2	3.35	3.36
	5	0.5	30	6.2	3.575	2.6	8.2	0	3.36
Transition Zone		Thickness of Transition Zone d (km)							
	6	0.2	29.9	6.2	3.575	2.6	8.2	4.73	3.36
	7	0.5	29.75	6.2	3.575	2.6	8.2	4.73	3.36
	8	1.0	29.0	6.2	3.575	2.6	8.2	4.73	3.36
	9	4.0	28.0	6.2	3.575	2.6	8.2	4.73	3.36
Lamina		Thickness of Lamina h (km)							
	10	1	30	6.2	3.575	2.6	8.2	4.73	3.36
	11	0.5	30	6.2	3.575	2.6	8.2	4.73	3.36
	12	0.25	30	6.2	3.575	2.6	8.2	4.73	3.36

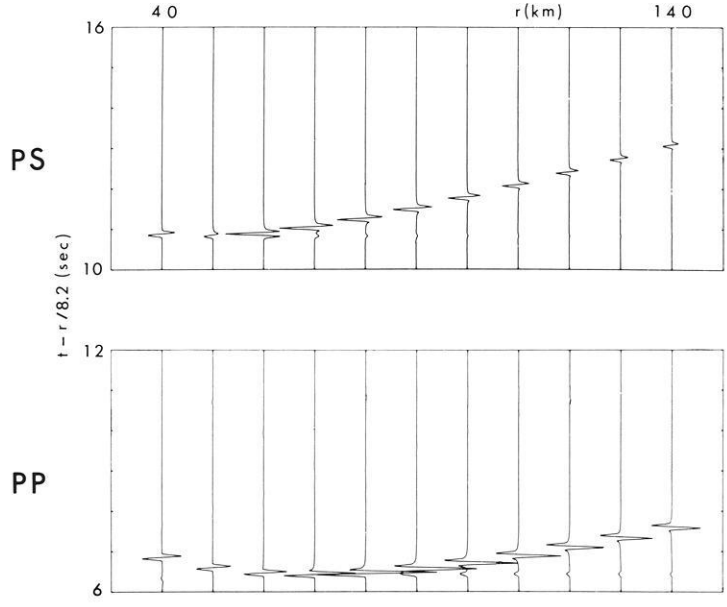

Fig. 6. Section of synthetic seismograms of *PP*- and *PS*-reflections from a first-order discontinuity at a depth of 30 km; vertical component, free surface reflection taken into account (model 1 in Table 1)

the following several possibilities for a reduction of *PS*-amplitudes are discussed. The most likely model is a transition zone, since *PS* coupling decreases in an inhomogeneous medium with decreasing gradients of the elastic properties. However, other reasons – variable Poisson's ratio in the upper mantle and reflection from a lamina – will be investigated as well.

3.2. PS-Reflections from a Linear Transition Zone

In the high-frequency limit of geometrical ray theory no converted *PS*-reflections are expected to arise from a transition zone in which the elastic parameters and the density change continuously with depth. However, for finite frequencies the equation of motion of an inhomogeneous medium does not separate completely in two wave equations for compressional and shear waves. The coupling between *P*- and *S*-waves is the stronger the larger the gradient of the elastic properties and density. Therefore, *PS*-reflections are to be expected also from continuous transition zones. Their amplitudes cannot be derived from geometrical ray theory.

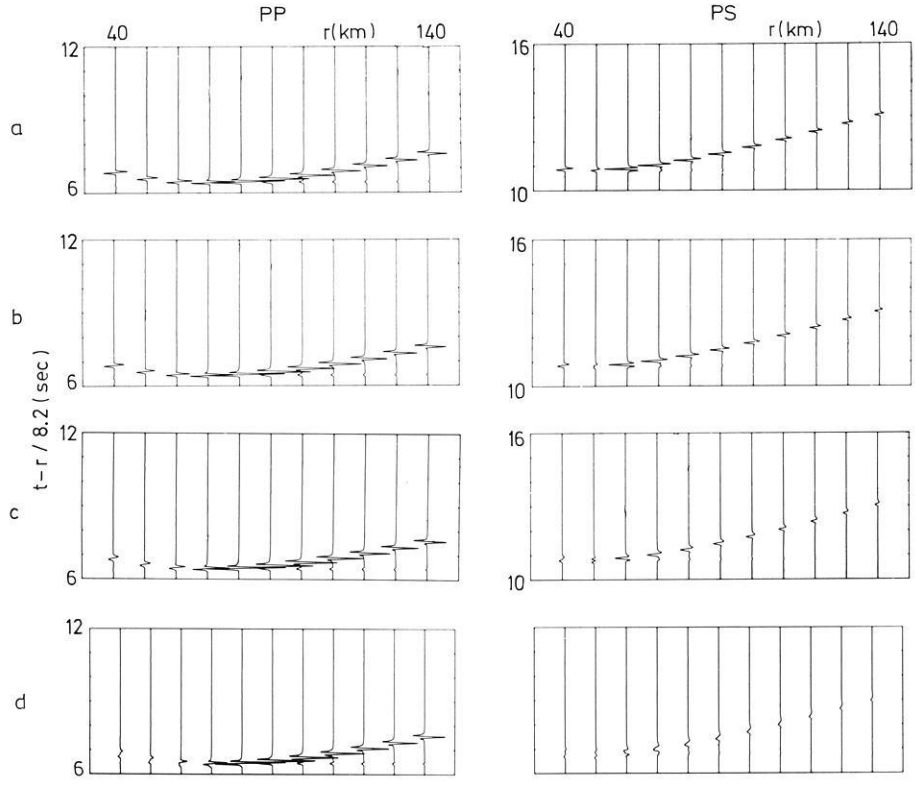

Fig. 7. Sections of synthetic seismograms of *PP*- and *PS*-reflections from linear transition zones of thickness $d = 0.2$ (b), 0.5 (c) and 1.0 km (d) (models 6 to 8 in Table 1) compared with section from first-order discontinuity (a). Vertical component, free surface accounted for

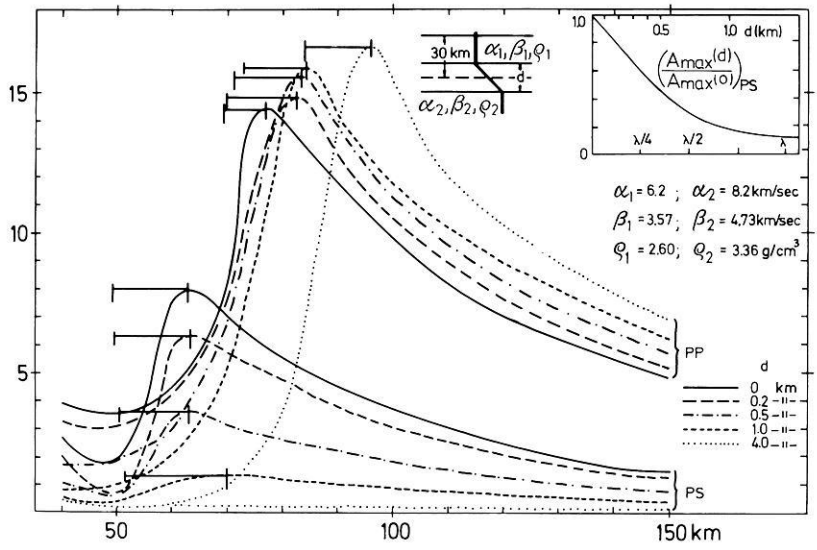

Fig. 8. Amplitude distance curves of *PP*- and *PS*-reflections from linear transition zones of thickness $d = 0$ (first-order discontinuity), 0.2, 0.5, 1.0 and 4.0 km. The displacements of the amplitude maxima from the critical distance are indicated. In the inlet the ratio of maximum *PS*-amplitudes to that from a first-order discontinuity are plotted as a function of thickness d of the transition zone and wavelength

In this section theoretical amplitudes will be computed with the aid of synthetic seismograms. The linear transition zone is approximated by a stack of 10 thin homogeneous layers. In Fig. 7 the *PP*- and *PS*-record sections of a first-order discontinuity are compared with those from transition zones of thickness 0.2 km to 1.0 km (models 6 to 8 in Table 1). As was expected, the amplitudes of supercritical *PP*-reflections are hardly changed by the introduction of the transition zone. Only the subcritical *PP*-reflections decrease strongly with increasing thickness of the transition zone. On the other hand, the *PS*-reflections diminish both in the sub- and supercritical distance range.

Amplitude-distance curves for transition models with thicknesses from 0 to 4.0 km are compiled in Fig. 8. The shift of the amplitude maxima relative to the critical points occurs also in case of transition zones and is indicated in the figure. The inlet in Fig. 8 gives the amplitude of the *PS* maxima as a function of transition thickness and *P*-wavelength ($\lambda = 1.4$ km). A rapid decrease of maximum amplitudes with growing thickness of the transition zone is to be noted. If the thickness equals about one wavelength, the maximum amplitude is only 1/10 of the maximum amplitude from a first-order discontinuity. If transition zones are considered to be responsible for the absence of *PS* phases in the observations, it suffices to replace the first-order discontinuity by transition zones of thickness of about one *P*-wavelength. – In turn it can be argued that if *PS*-reflections should be observed their presence would have to be taken as evidence of an extremely sharp transition zone of thickness less than one wavelength.

3.3. PS-Reflections from a First-Order Discontinuity with Variable Poisson's Ratio in the Lower Half-Space

It has been pointed out already that a transition zone is not the only possible explanation of the absence of *PS*-reflections. Even in case of a first-order discontinuity the ratio of *P*- to *S*-wave velocities may drastically change the amplitudes of the reflected *PS*-waves. In this section we will change the Poisson's ratio σ in the lower half-space from 0.25 to 0.5 keeping this ratio constantly 0.25 in the upper half-space. This range would correspond to a gradual transition from a solid through a partially molten lower half-space to a fluid medium.

In Fig. 9 a comparison of synthetic *PP*- and *PS*-record sections is given for $\sigma = 0.25$, 0.30, 0.378, 0.5 (models 1 to 5 in Table 1). While the amplitudes of the supercritical *PP*-reflections hardly change, the amplitudes of the supercritical *PS*-reflections are affected strongly. They decrease with increasing Poisson's ratio. The case $\sigma = 0.378$ and equal density in both media corresponds to equal *S*-wave velocity in which case no *PS*-waves are generated at the interface since here compressive and shear motions decouple completely (this case is a very efficient

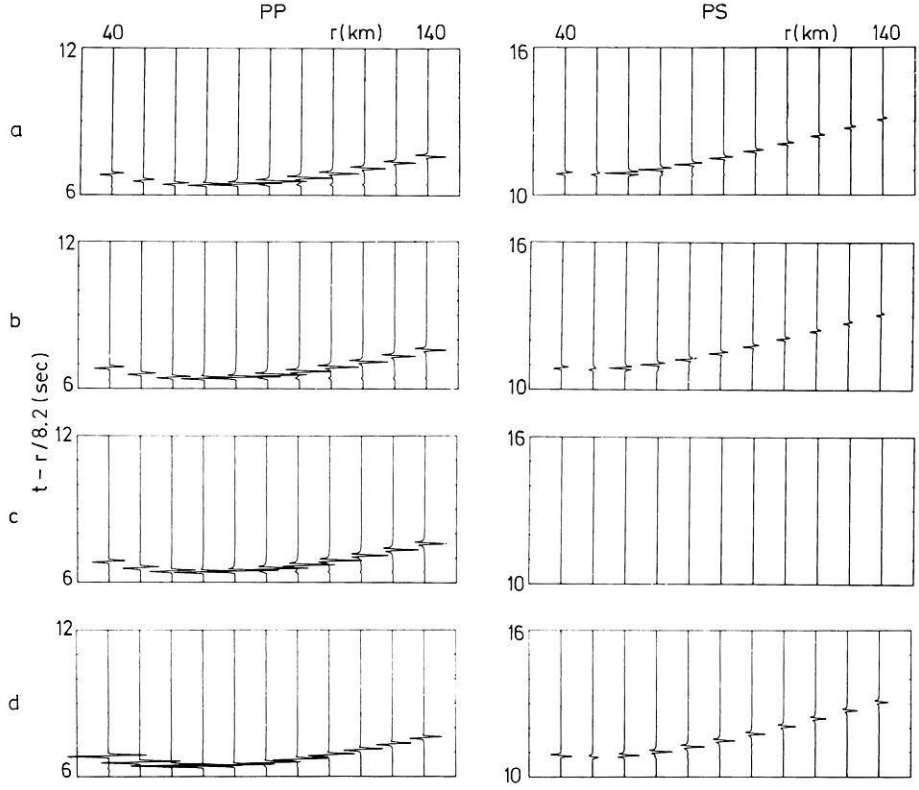

Fig. 9. Sections of synthetic seismograms of *PP*- and *PS*-reflections from a first-order discontinuity with variable Poisson's ratio in the lower halfspace ($\sigma = 0.25$ (a), 0.30 (b), 0.378 (c), 0.5 (d), models 1 to 5 in Table 1); vertical component free surface accounted for. For $\sigma = 0.378$ the density in both halfspaces has been chosen equally as 2.6 g/cm^3; complete decoupling of compressional and shear waves

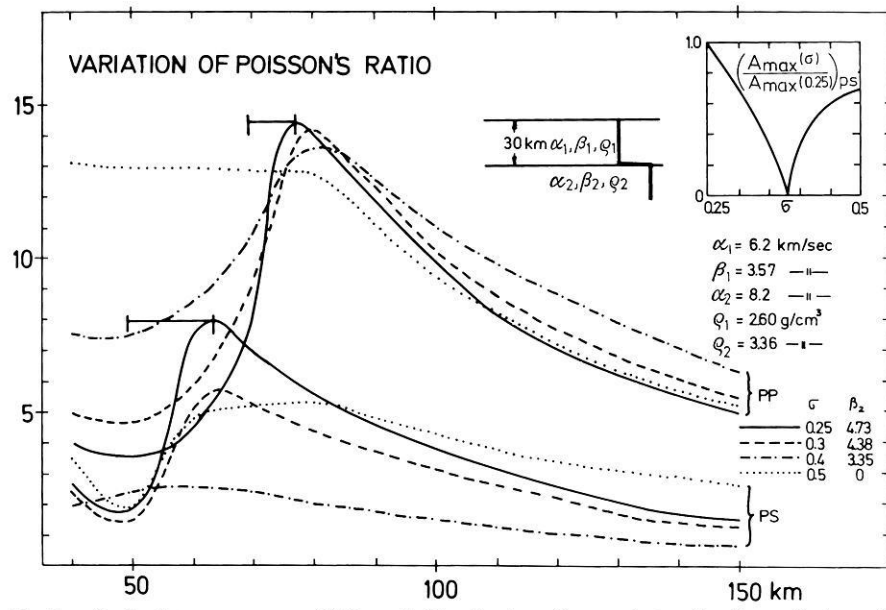

Fig. 10. Amplitude distance curves of *PP*- and *PS*-reflections from a first-order discontinuity with variable Poisson's ratio σ in the lower halfspace ($\sigma = 0.25, 0.3, 0.4, 0.5$). In the inlet the ratio of maximum *PS*-amplitudes to that for $\sigma = 0.25$ is plotted as a function of σ

test of the computer-program). For $\sigma > 0.378$ the amplitudes of the *PS*-reflections increase again but do not reach the amplitudes of the case $\sigma = 0.25$. Amplitude-distance curves for $\sigma = 0.25$, 0.3, 0.4 and 0.5 are compiled in Fig. 10. The inlet of this figure gives the ratio of the maximum *PS*-amplitude to that with $\sigma = 0.25$ as a function of σ. It is quite evident that a reduction of the *S*-wave velocity in the lower half-space can also be the cause for the disappearance of *PS*-reflections.

3.4. PS-Reflections from Single Laminas with Variable Thickness

The amplitudes of the supercritical reflection from a high velocity layer diminish substantially if the layer is thin enough and embedded between two low velocity half-spaces. For the sake of brevity, such a layer will be termed a lamina. If the lamina is sufficiently thin, the supercritical reflection looses energy since a considerable part of it is leaking through the lamina into the lower half-space. It is not known so far whether the supercritical *PS*-reflections are as strongly affected by this leakage as the *PP*-reflections.

In Fig. 11 sections of synthetic seismograms of *PP*- and *PS*-reflections from a lamina of variable thickness $d = 1.0$, 0.5 and 0.25 km are compared with the reflections from a first-order discontinuity. Both headwaves *PPP* and *PPS* have disappeared. One recognizes that the maximum amplitudes of both *PP*- and *PS*-waves diminish with decreasing thickness of the lamina. The amplitude-distance curves for these cases are presented in Fig. 12.

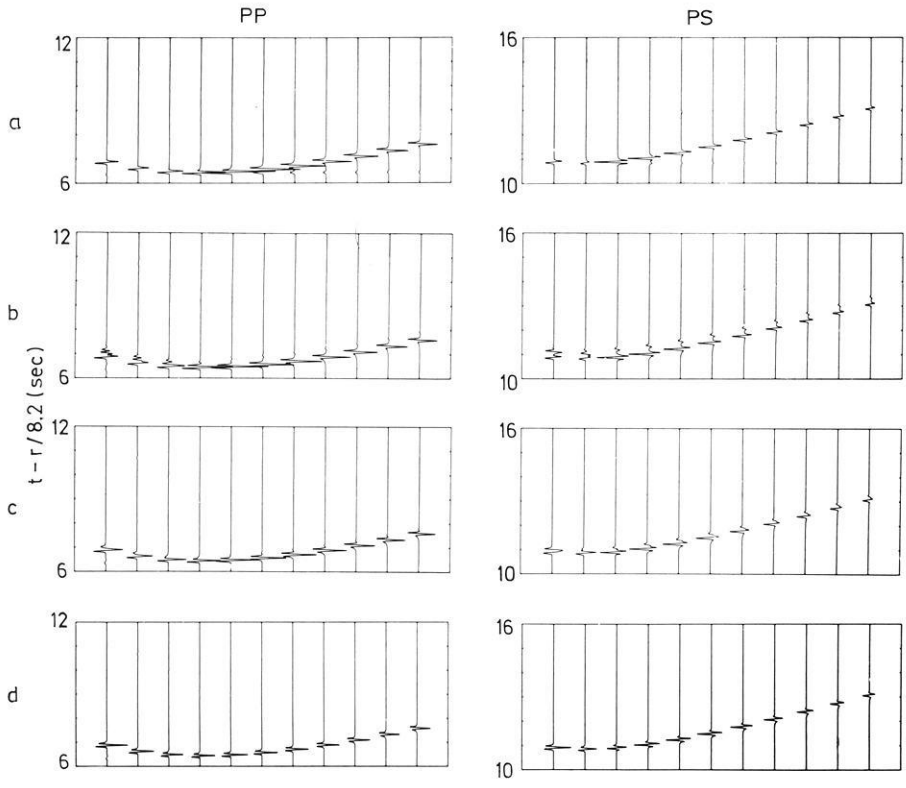

Fig. 11. Sections of synthetic seismograms of *PP*- and *PS*-reflections from a lamina with variable thickness $h = 1.0$ (b), 0.5 (c) and 0.25 km (d) (models 10 to 12 in Table 1) between two low velocity halfspaces compared with reflections from a first-order discontinuity (a); vertical component, free surface accounted for

It is obvious that the supercritical *PP*-reflections decrease much more rapidly in amplitude than the *PS*-reflections. For $d = 0.25$ km both types of reflections show nearly equal maximum amplitudes. The behaviour of the maximum amplitudes is summarized in the inlet of Fig. 12 as a function of layer thickness. It may be concluded that the *PS*-reflections from a thin lamina are less affected by the leakage of energy into the lower half-space than the *PP*-reflection. Therefore a single lamina is no suitable model for the explanation of the observed absence of *PS*-reflections from the crust-mantle boundary.

4. Discussion and Conclusions

In the first part of this paper the expressions for the *PS*-reflections from transition zones with arbitrary depth distributions of the elastic moduli and density have been derived. The program "Reflexion" described previously in detail by Fuchs and Müller (1971) has been extended to include the computation of synthetic

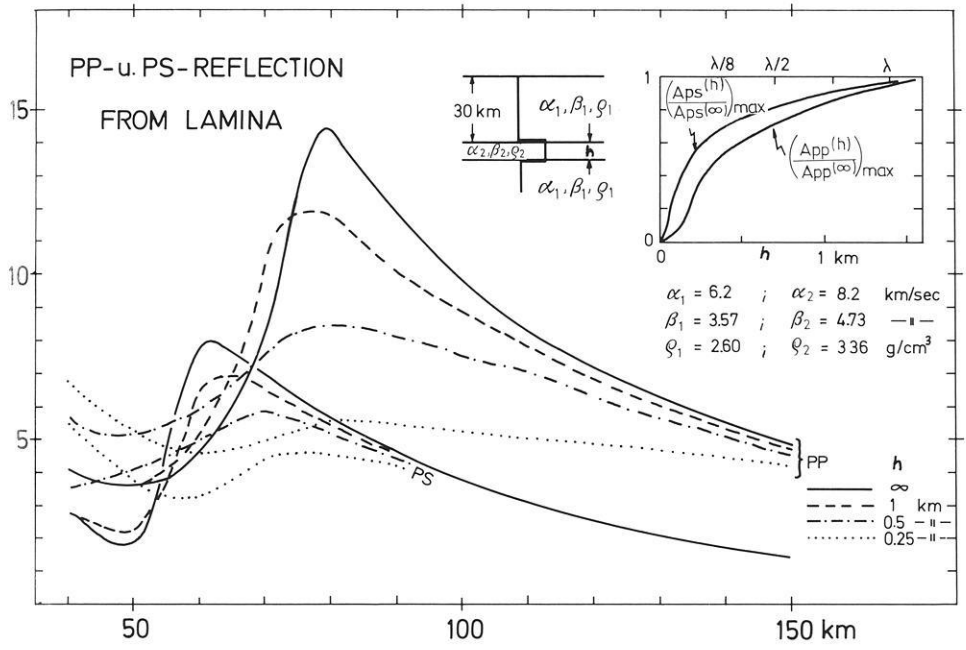

Fig. 12. Amplitude distance curves of *PP*- and *PS*-reflections from a lamina with variable thickness $h = 1.0$, 0.5 and 0.25 km. In the inlet the maximum *PP*- and *PS*-amplitudes to that for the first-order discontinuity is plotted as a function of thickness of the lamina and of the wavelength

PS-reflections. The extended program has been applied to a problem encountered in explosion seismology, *i.e.* the absence of *PS*-reflections converted at the crust-mantle boundary in the presence of strong *PP*- and *SS*-reflections.

Firstly, it could be shown that *PS*-reflections from a first-order discontinuity model of the crust-mantle boundary with Poisson's ratio $\sigma = 0.25$ should possess amplitudes comparable in size with those of the *PP*-reflection. Such a model is not in accordance with the observations. Therefore, reflections from linear transition zones have been investigated which in fact cause a strong diminution of *PS*-amplitudes with increasing thickness of the transition zone while *PP*-amplitudes show no decrease in the supercritical distance range. A thickness of about one wavelength reduces the maximum *PS*-amplitudes to 1/10 of their size for a first-order discontinuity, *i.e.* already a very thin transition zone with thickness more than 1 km will cause the *PS*-reflections to become unobservable. Therefore, supercritical *PS*-reflections are a very sensitive indication of the presence of first-order discontinuities. Wherever models with first-order discontinuities are postulated *PS*-reflections should be observable. So far, no *PS*-reflections from the crust-mantle boundary are known to the author. Should there exist regions where *PS*-reflections can be observed, the crust-mantle boundary must be extremely sharp.

A variation of Poisson's ratio in the upper mantle below the crust-mantle boundary is another possible cause for the suppression of *PS*-reflections. If, by partial melting, the *S*-velocity and density become equal to the *S*-velocity and

density in the overburden, *PS*-reflections may completely disappear. Thin Laminas diminish the amplitudes of *PP*-reflections more strongly than those of *PS*-reflections. Therefore, they do not provide an explanation of the observed phenomenon.

From the present study a variation of Poisson's ratio or the existence of a transition zone seem to be the only possible causes for the absence of *PS*-reflections. Since the variation of the Poisson's ratio would require a substantial partial melting immediately below the crust-mantle boundary, the author tends to explain the absence of *PS*-reflections by the existence of a transition zone. It must be concluded that the transition zone at the crust-mantle boundary must have a thickness of more than 1 km. From this study a search for *PS*-reflections on crustal record sections is recommended.

Acknowledgements. The author is indebted to Drs. G. Müller and C. Prodehl for many fruitful discussions and kindly reading the manuscript and to Dr. K.-O. Millahn for help in the computation. This work is sponsored by the Deutsche Forschungsgemeinschaft. Computing facilities were made available by the computer center of Karlsruhe University.

References

Berry, M.J., Fuchs, K.: Crustal structure of the Superior and Greenville provinces of the northeastern Canadian shield. Bull. Seism. Soc. Am. **63**, 1393–1432 (1973)

Červený, V.: The amplitude curves of reflected harmonic waves around the critical point. Studia geophys. geodaet. **5**, 319–351 (1961)

Fuchs, K.: Das Reflexions- und Transmissionsvermögen eines geschichteten Mediums mit beliebiger Tiefen-Verteilung der elastischen Moduln und der Dichte für schrägen Einfall ebener Wellen. Z. Geophys. **34**, 389–413 (1968a)

Fuchs, K.: The reflection of spherical waves from transition zones with arbitrary depth-dependent elastic moduli and density. J. Phys. Earth **16**, (Special Issue), 27–41 (1968b)

Fuchs, K., Müller, G.: Computation of synthetic seismograms with the reflectivity method and comparison with observations. Geophys. J.R.A.S. **23**, 417–433 (1971)

Kaminski, W., Fuchs, K., Menzel, H.: Crustal investigations along a seismic refraction line from the Harz mountains to the Alps, Paper IASPEI-166, presented at the 14th General Assembly IUGG, Zürich, 1967

Müller, G.: Theoretical seismograms for some types of pointsources in layered media, Part I: Theory. Z. Geophys. **34**, 15–35 (1968a)

Müller, G.: Theoretical seismograms for some types of pointsources in layered media, Part II: Numerical calculations. Z. Geophys. **34**, 147–162 (1968b)

Müller, G.: Exact ray theory and its application to the reflection of elastic waves from vertically inhomogeneous media. Geophys. J.R.A.S. **21**, 261–283 (1970)

Müller, S., Prodehl, C., Mendes, H.S., Moreira, V.S.: Crustal structure in the southwestern part of the Iberian peninsula. Tectonophysics **20**, 307–318 (1973)

Prof. Dr. K. Fuchs
Geophysikalisches Institut der Universität
D-7500 Karlsruhe-West
Hertzstraße 16
Federal Republic of Germany

Received March 17, 1975